



A wind turbine driven hybrid HDH-MED-MVC desalination system towards minimal liquid discharge

Saeed Rostami ^a, Hamed Ghiasirad ^{b,*}, Hadi Rostamzadeh ^a, Ali Shokri Kalan ^c, Abbas Maleki ^d

^a Department of Aerospace Engineering, Sharif University of Technology, Azadi Ave., Tehran, Iran

^b Silesian University of Technology, Faculty of Energy and Environmental Engineering, Department of Power Engineering and Turbomachinery, ul. Konarskiego 18, 44-100 Gliwice, Poland

^c Department of Mechanical Engineering, Sahand University of Technology, Sahand New Town, Tabriz, Iran

^d Department of Energy Engineering, Sharif University of Technology, Azadi Ave., Tehran, Iran

ARTICLE INFO

Keywords:

Waste heat
Wind turbines
Desalination
HDH-MED-MVC
Energy analysis
Exergy analysis

ABSTRACT

Global issues arising from water and electricity shortages have notoriously affected social life over the last decades. In this regard, using renewable energy sources like waste heat of wind turbines (WTs) to drive desalination systems can be a promising solution. However, high specific work consumption (SWC) for desalinating seawater from the waste heat of the wind turbine generator can hinder the application of this new emerging technology. To address this problem, a multi-effect distillation mechanical-vapor compression (MED-MVC) desalination unit is used to recover the brine rejected from a humidification-dehumidification (HDH) desalination unit operating by the waste heat of the generator of a wind turbine. To reduce the rejected brine, 90% of the rejected brine is added to the mainstream of the HDH desalination system. The devised system is evaluated in terms of the first and second laws of thermodynamics using engineering equation solver (EES) software. The proposed cycle with a seven-effect MED-MVC unit has a lower SWC than the same cycle with a reverse osmosis (RO) unit. It is noteworthy the freshwater rate increases by 18% at all wind speeds. Parametric study shows the SWC decreases from 33.41 to 21.27 kWh/m³ by enhancing the wind speed.

1. Introduction

The profound effects of water and energy on the quality of the modern lifestyle can hardly be denied. Water scarcity can be originated from varied reasons, including but not limited to economic barriers, management failure, climate change, geographical features, and political disputes (Rostamzadeh and Rostami, 2020a). In Iran, large areas, particularly in the eastern and southern parts of the country, are experiencing severe dryness (Iranian Meteorological Organization (IMO), 2018). On the other hand, energy is one of the vital parameters for sustainable community development as it is a prerequisite for continuous water supply. Energy shortages stem from the increasing demand to supply chain lack of continuous investment, low power plant efficiency, contradictory upstream policies, and, more importantly, environmental constraints. Therefore, one of the most important questions arising between the academics and production niches is how to provide a viable, sustainable, and economical co-supply of water and energy for sustainable societies. Innumerable works have been conducted over the

last decades in terms of the water-energy nexus concept, and valuable solutions are presented accordingly to tackle this dilemma. Regarding water shortage in the vicinity of open seas, seawater desalination is one of the best remedies to overcome the water scarcity issue since more than 97% of the earth's water is found in the form of saline water in seas and oceans (Kalogirou, 2005). On the other side, renewable energies are unanimously recommended as the best solution to overcome future energy shortages as they produce significantly lower greenhouse gasses, reduce dependence on fossil fuels, and diversify the energy supply chain, to exemplify a few. International Energy Agency (IEA) has prognosticated widespread use of renewable energies is expected to address the 99% rise in the global electricity demand between 2020-2025 (International Energy Agency, 2020). Hence, investing in renewable energy-based seawater desalination technologies via either thermal or mechanical mechanisms such as humidification-dehumidification (HDH), multi-effect distillation (MED) (Rostamzadeh et al., 2019), and reverse osmosis (RO (Fairuz et al., 2023), should be considered by this time.

A thermal vapor compression (TVC) unit plays a vital role in terms of

* Corresponding author.

E-mail address: Hamed.Ghiasirad@polsl.pl (H. Ghiasirad).

<https://doi.org/10.1016/j.sajce.2023.03.007>

Received 4 August 2022; Received in revised form 23 February 2023; Accepted 30 March 2023

Available online 31 March 2023

1026-9185/© 2023 The Authors. Published by Elsevier B.V. on behalf of Institution of Chemical Engineers. This is an open access article under the CC BY license (<http://creativecommons.org/licenses/by/4.0/>).

Nomenclature Abbreviations	
<i>Symbols</i>	
C_p	Specific heat at constant pressure (kJ/kg.K)
BFR	Brine Flow Ratio
EES	Engineering Equation Solver
\dot{E}_n	Energy rate (kW)
ERT	Energy recovery turbine
ex	Exergy per unit mass (kJ/kg)
\dot{E}_x	Exergy rate (kW)
GOR	Gained Output Ratio
h	Specific enthalpy (kJ/kg)
\dot{H}	Enthalpy rate (kW)
HDH	Humidification-Dehumidification
h_{fg}	Enthalpy of vaporization (kJ/kg)
HPP	High-pressure pump
M	Molar mass (kg/kmol)
\dot{m}	Mass flow rate (kg/s)
MED	Multi-effect desalination
Mix	Mixer
MR	Mass ratio of HDH desalination
MVC	Mechanical Vapor Compression
N	Number of effects
P	Pressure (bar)
PC	Performance coefficient
PR	Performance Ratio
\dot{Q}	Heat transfer rate (kW)
R	Global gas constant (kJ/kg.K)
RO	Reverse osmosis
s	Specific entropy (kJ/kg.k)
S	Salinity (g/kg)
sal	Salinity (g/kg)
SWC	Specific work consumption (kWh/m ³)
T	Temperature (k)
TTD	Terminal temperature difference (K)
u	Wind velocity (m/s)
u_c	Cut-in speed (m/s)
u_r	Rated speed (m/s)
\dot{W}	Power (kW)
\dot{W}_{avg}	Average Power (kW)
X	Salinity (g/kg)
z	Height (m)
<i>Subscripts and superscripts</i>	
a	Air
avg	Average
ch	Chemical
Comp	Compressor
c.v.	Control volume
D	Destruction
Da	Dry air
Eff	Effect
Ex	Exergy
F	Furling
Fu	Fuel
FW	Freshwater
gear	Gearbox
gen	Generator
Hum	Humidifier
Dhum	Dehumidifier
i	ith stream
In	Inlet
is	isentropic
isen	isentropic
K	Kth component
L	Loss
M	Maximum
Net	Net value
out	Outlet
Ph	Physical
Pr	Product
pum	Pump
R	Rated
RHX	Recovery Heat Exchanger
Sw	Sea Water
tot	Total
v	Vapor
WT	Wind Turbine
WH	Waste heat
1,2,3,...	Number of streams
0	Dead State
<i>Greek symbols</i>	
B	Velocity and altitude coordinator (constant parameter)
Δ	Difference
ε	Effectiveness (%)
η	Efficiency (%)
ω	Humidity ratio
ρ	Density (kg/m ³)
Γ	Gamma function
ϕ	Relative humidity

providing a continuous supply of high-temperature and pressure steam for MED systems. However, it is normally recommended for occasions with direct access to large-scale power plants that can partially bypass the high turbine backpressure steam towards the primary entrance of the TVC. In areas without the possibility of providing high-pressure and temperature steam, mechanical vapor compression (MVC) can be considered as a proportionate alternative (Rostamzadeh, 2021). Compared to MED-TVC desalination systems, MED-MVC units provide high-quality freshwater, continuous operation at decentralized regions, compact and uncomplicated set-up, stable operation, and a simple mechanism to be connected to renewable energies, and low economical operating (Elsayed et al., 2019a). Moreover, the production capacity and brine level in the MVC-TVC systems are extremely sensitive to a minor variation in the inlet seawater temperature (Elsayed et al., 2018). A MED-MVC unit can be found in four different configurations: parallel-cross feed (PCF), parallel feed (PF), forward feed (FF), and

backward feed (BF). Under the same conditions, the maximum exergetic and energetic performances belong to PCF configuration (Elsayed et al., 2019b; Jamil and Zubair, 2018; Rostamzadeh, 2021). These configurations can be structured in terms of single-effect or multi-effect mechanisms. The SWC of a single-effect MVC (SE-MVC) unit can be as high as 10–13 kWh/m³ (Jamil and Zubair, 2017a). In general, the SWC of a SE-MVC unit can be decreased once its mechanism is changed into MED-MVC (Jamil and Zubair, 2017b). However, more specifically, the amount of decrease in the SWC of a MED-MVC unit is highly contingent upon its structure and key design parameters. For instance, for a MED-MVC unit with PCF configuration and under a similar design condition proposed in this study, Rostamzadeh et al. (Rostamzadeh et al., 2020) recommended a MED-MVC desalination unit with seven effects as the optimal structure. They reported SWC as low as 8.29 kWh/m³. Later, Rostamzadeh (Rostamzadeh, 2021) proposed a new configuration instead of the previously proposed MED-MVC unit with

the same number of effects and found that the SWC can be decreased by 25.45%. Therefore, to follow the self-consistency of the open literature, the same number of effects (i.e., seven effects) are selected for the MED-MVC unit.

Over the last decade, the use of thermal heat dissipated by renewable energy-based technologies, especially wind turbines, has received great attention. Like the waste heat captured from other industrial sectors for by-products applications (Ghorbani et al., 2020; Zaitsev et al., 2020), the waste heat dissipating from the wind turbine generator can also be used for diverse applications due to its significant contribution to waste-to-product purposefully. Wind thermal energy has the potential to become an economical and reliable energy source despite its fledgling establishment (Okazaki et al., 2015). Following recent advances in the open literature, a great focus of attention is drawn to the emerging concept of multi-generation applications. For instance, in terms of waste-to-electricity applications, by accounting for the waste thermal heat of the generator of the wind turbines, Karasu and Dincer (Karasu and Dincer, 2018) devised a wind thermal energy storage (WTES) system combined with molten salt storage for further electrical power production from the dissipated thermal energy of the wind turbine's generator by employing an organic Rankine cycle (ORC). They applied thermodynamic tools to evaluate the performance of the devised system and reported exergy and energy efficiencies of around 8.6% and 7%, respectively. In another similar study, Nematollahi et al. (Nematollahi et al., 2019) set up a new system, including an ORC and a wind turbine, for using the waste heat of the wind turbine generator. They used thermo-economic and thermodynamic approaches to evaluate the performance of the proposed integrated system. They screened seven different working fluids to investigate their effects on the performance and cost metrics. Their results showed that R134a can lead to the highest power of 7.1 kW, while the lowest of 6.25 kW can be generated when SES36 is used. For trigeneration applications, Khalilzadeh and Nezhad (Khalilzadeh and Hossein Nezhad, 2020) proposed a new system for simultaneous power, heating, and cooling supply of a sustainable community by extracting waste heat from 12 wind turbines with a nominal power capacity of 7500 kW. To achieve this goal, they combined absorption refrigeration and ORC. The devised system had exergy and energy efficiencies of 38.61% and 45.32%, respectively. Rostami et al. (Rostami et al., 2021) designed a novel integrated system to capture the waste heat of a wind turbine for cooling and freshwater production. The authors used an absorption chiller driven by the dissipated thermal heat of the wind turbine and produced water from the available moisture in the air instead of desalinating seawater. The authors have expanded the simulation results for two windy and humid areas in Iran. The investigation results showed that Cu/water and TiO₂/water mixtures have the highest and the lowest performances, respectively. For seawater desalination applications via the wind turbine waste-to-freshwater concept, Memon et al. (Memon et al., 2022a) studied four different configurations for multi-stage contact membrane distillation units driven by the waste heat of a wind turbine for freshwater production. Configurations proposed by authors included a parallel with 15 × 1 module, a series with 1 × 15 modules, a parallel series with 5 × 3 modules, and a parallel series with 3 × 5 modules. They found that the second configuration (i.e., a series with 1 × 15 modules) can produce more freshwater in the capacity range of 1927–10158 kg/h than the other ones. However, for achieving the highest GOR, it is more appropriate to use the fourth configuration (i.e., a parallel series with 3 × 5 modules). Rostamzadeh and Rostami (Rostamzadeh and Rostami, 2020b) proposed a new system for driving an HDH unit using the dissipated heat of a wind turbine to produce freshwater. The devised system was investigated from the first and second laws of thermodynamics and showed that the freshwater rate, Gain-Output-Ratio (GOR), and net power increase with the rise of wind speed while the exergy efficiency shows an opposite trend through this alteration. Khalilzadeh and Nezhad (Khalilzadeh and Hossein Nezhad, 2018) used the waste heat from the generator of a wind turbine to drive a MED system. They analyzed the devised system from energy, exergy,

and thermo-economic points of view. They employed a wind turbine with a nominal capacity of 7580 kW and produced 45.06 m³/day freshwater with the cost of 16.676 \$/m³ at the wind speed of 11 m/s. More recently, Rostamzadeh et al. (Rostamzadeh et al., 2021) compared the performance and cost metrics of the hybrid HDH-RO desalination unit driven by waste thermal heat and mechanical power of the wind turbine with the RO unit driven only by the electrical power of the wind turbine. Their results indicated that the hybrid HDH-RO desalination unit suffers from high operating and maintenance costs relative to the RO unit. The authors generalized their conclusion by conducting the study for six different wind turbines of E-101/3.5, V-115/4.1, G-128/4.5, GW-136/4.8, Eno-114/4.8, and AD-116/5. They also reported that GW-136/4.8 has the highest exergy efficiency at low wind speed (lower than 9 m/s), followed by AD-116/5. To follow up this conclusion, the same wind turbine model (i.e., GW-136/4.8) is selected for the system. Moreover, Lawal et al. (Lawal et al., 2021) integrated a multi-stage flash (MSF) desalination unit with an HDH bottoming cycle to achieve a GOR of 8.73. This way, the HDH unit can provide drinking water for 134,000 people consuming 5 L/day. After that, Memon et al. (Memon et al., 2022b) exploited the waste heat of a wind turbine for a multi-stage direct contact membrane desalination (DCMD) for which they noticed that the series-parallel configuration is the optimized one when designing 3 × 5 modules to have a high value of GOR. Then, Tahir and Al-Ghamdi (Tahir and Al-Ghamdi, 2022) analyzed an integration of MED-HDH-ZLD desalination systems in which the topping cycle is MED. At the end of the process, an evaporative crystallizer is installed to separate the brine and salt. Their parametric study results show that higher top temperatures lead to a rise in performance ratio from 9 to 12.

1.1. Scientific gap

According to the above reviewed literature it can be fathomed out that there are several scientific gaps in the existing previous studies dealing with waste heat recovery of wind turbines for freshwater supply. For example, it has been shown that using a RO unit as a bottoming cycle of an HDH system driven by the waste heat of a wind turbine significantly increases the SWC of the desalination plant (Rostamzadeh et al., 2021). A high value for the SWC of the HDH-RO unit can result in high operating costs for the freshwater, as underlined by Khalilzadeh and Nezhad (Khalilzadeh and Hossein Nezhad, 2018). In fact, Khalilzadeh and Nezhad (Khalilzadeh and Hossein Nezhad, 2018) reported a high value of 16.16 \$/kWh and 125 kWh/m³ for the freshwater cost and SWC, respectively when a MED unit was employed to capture the waste heat of the generator of the wind turbine. It is obvious that the freshwater produced from a MED unit is more expensive than that of an HDH unit due to a high purchased equipment cost of the MED desalination systems. In addition, the HDH-RO unit proposed by Rostamzadeh et al. (Rostamzadeh et al., 2021) cannot be transformed to brine reduction systems by employing brine recycling scheme since the salinity of the discarded brine streams is so high. Such high amount of highly concentrated saline water to the environment can provoke various irrecoverable environmental issues. Since a MED unit normally discards brine at a relatively elevated temperature, the rate of exergy loss associated with the discarded brine is high. Therefore, these kinds of obstacles can be tackled by creating new ideas toward improving the structure of the previously proposed desalination systems driven by the waste heat of wind turbines.

1.2. Novelty

After noticing the above-mentioned scientific gaps, it can be figured out that integrating a thermal desalination unit instead of RO unit (albeit with the same capacity) into the HDH unit can significantly reduce the SWC and raise the freshwater capacity. Such structural modification can have more pronounced influence once minimal liquid discharge concept is also included to the preliminary stage of the design. In conclusion,

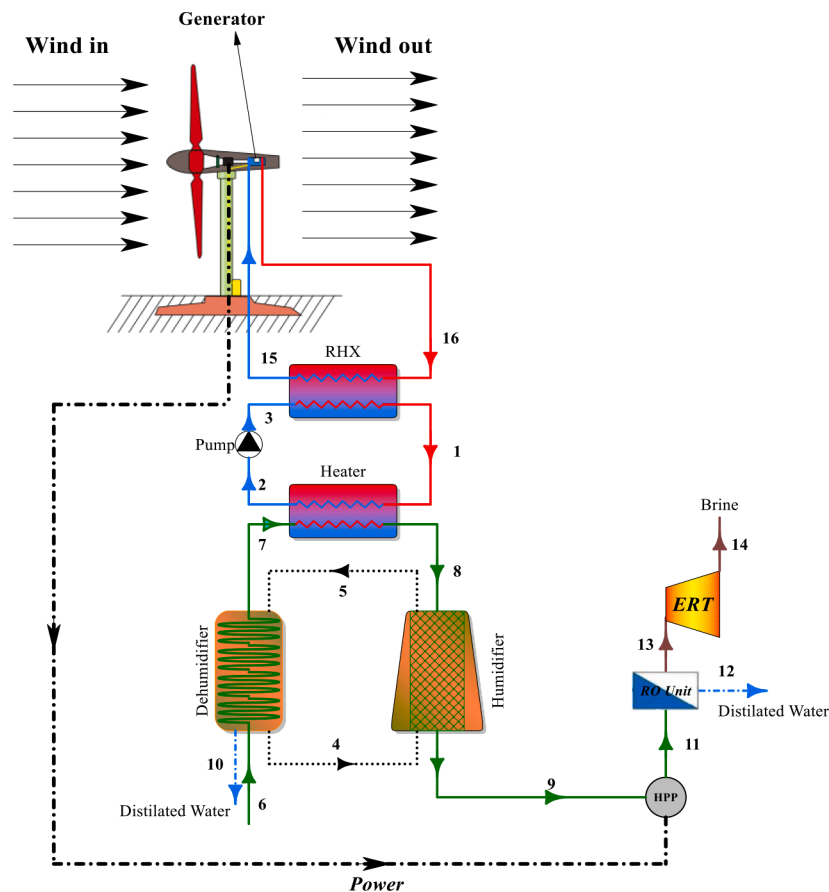


Fig. 1. Schematic of the reference system driven by waste heat and the electrical power of a wind turbine (Rostamzadeh et al., 2021).

taking advantage of an MED unit as a bottoming cycle of an HDH unit for waste heat recovery from the generator of the wind turbine leads to a high freshwater rate compared to an HDH unit. In addition, due to the low-temperature characteristics of the waste thermal energy extracted from a wind turbine, the use of this dissipated heat to drive an HDH unit on the top is more consistent as the irreversibility of the components associated with the HDH unit is lower. Because of a large amount of liquid discharge of the MED system, it is necessary to overcome such deficiency by proposing a minimal liquid discharge concept. Hence, the present study seeks to not only lessen the SWC of the HDH unit driven by the waste heat of the generator of the wind turbine via recovering its discarded brine via a MED-MVC unit but also reduce the rejected brine from the hybrid HDH-MED-MVC unit for sustainable development. To decrease the amount of SWC of the HDH system driven by the waste heat of the generator of a wind turbine, hybridization with a MED-MVC unit in a new structure is proposed. It is obvious that freshwater costs can be lessened by decreasing the SWC because the size of compressor is minimized. As mentioned in Ref. (Ghiasirad et al., 2021a), increasing the seawater temperature makes the system inefficient in water-heated HDH units, whereas most of the previous works such as (Ghofrani and Moosavi, 2020) added the warm brine to inlet seawater. In the present study, however, it is recirculated to seawater entering the heater, which can be considered as another novelty. Finally, there is no need for two conventional heat exchangers (water and brine coolers) in MED system contributing to decreasing the component's costs as well. In the proposed cycle, to achieve the lowest SWC, the best number of effects is found. To modify the structure of the proposed hybrid HDH-MED-MVC unit, a mechanism with brine reduction is designed. To discuss the advantages of the developed configuration, present study is compared to the HDH unit, RO unit, and hybrid HDH-RO unit. To prove the feasibility of the suggested co-generation system, the thermodynamic analysis is

done. To analyze the effect of sensitive variables, an all-inclusive parametric study is done.

2. Set-up description

Figs. 1 and 2 show the schematic of the reference system initially proposed in our previous study (Rostamzadeh et al., 2021) as well as the proposed hybrid HDH-MED-MVC unit, respectively. Detailed analysis and description of the reference system can be found in the related study; hence, any explanation about its operating mechanism is excluded here.

Fig. 2 displays the new proposed HDH-MED-MVC unit. The proposed system consists of three subsystems: a waste heat recovery sub-unit of the wind turbine (WT), an HDH desalination system, and a MED-MVC system. The waste heat recovery sub-unit of the wind turbine transfers thermal energy to the bottoming cycle (namely the HDH unit) while directly producing electricity from its wind turbine module. The waste heat recovery sub-unit of the WT includes three main components: a WT module, a recovery heat exchanger (RHX), and a pump. While being pressurized in the pump, the water stream at state 4 goes to RHX, where it has already been heated by the generator of the wind turbine and is quite ready to provide the required thermal energy. After passing through the RHX, the water stream enters the heater and provides an appropriate level of thermal energy required by the HDH desalination subsystem. The HDH desalination sub-system includes a humidifier, a dehumidifier, and a heater. As shown in Fig. 2, the water stream flows through an open loop, whereas the air flows in a closed loop, and this is exactly why this type of HDH desalination system is known as a closed-air open-water HDH cycle. After passing through the dehumidifier, seawater mixes with 90% of the brine rejected from the MED-MVC subsystem to build a stream with higher salinity than the reference

turbine (Rostamzadeh et al., 2021).

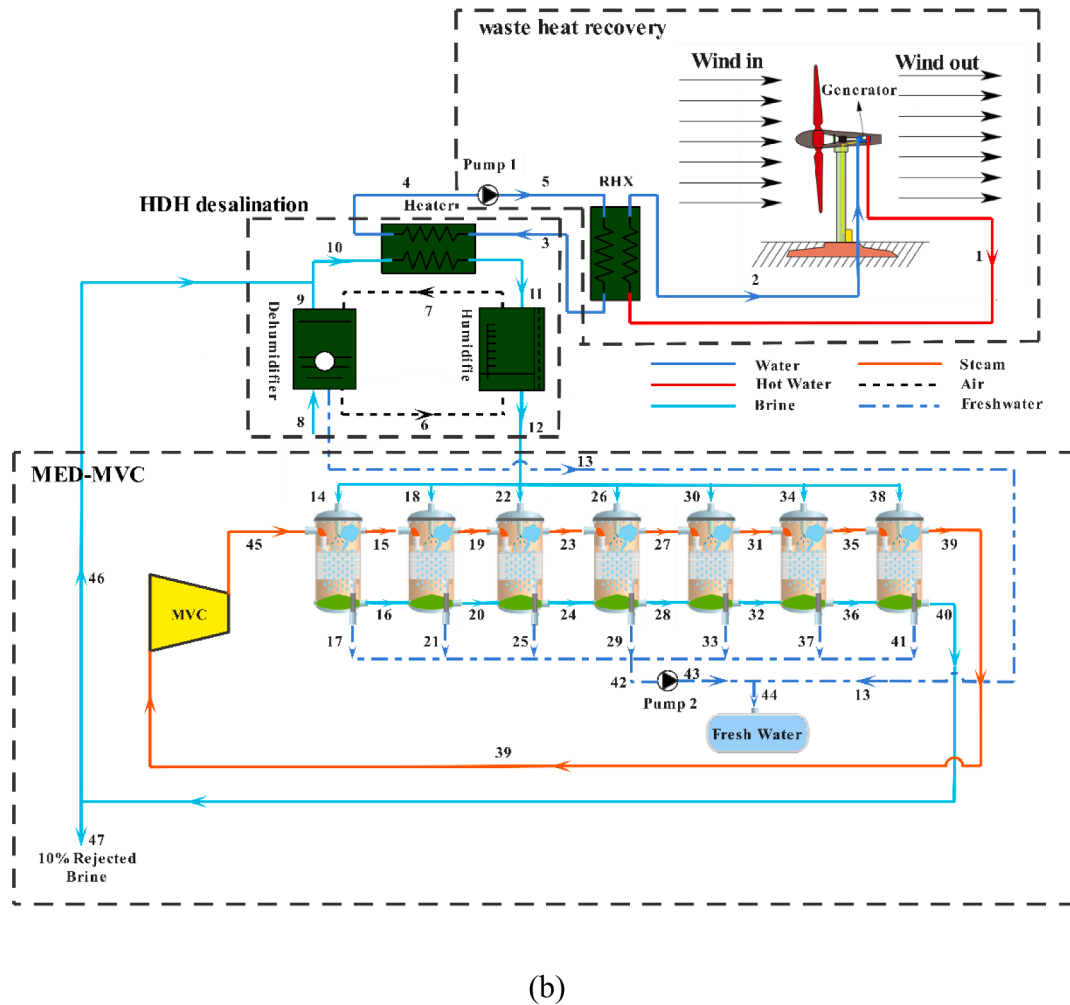


Fig. 2. The devised hybrid WT/HDH-MED-MVC system driven by waste heat and the electrical power of a wind turbine.

seawater. The MED-MVC sub-system, used to extract more freshwater from the brine rejected from the HDH sub-system, contains seven effects, a pump, a mixer, and a vapor compressor. The saturated vapor flows into a mechanical vapor compressor (MVC) while compressing and superheating the steam. To provide a better heat transfer mechanism, the brine is sprayed into the effect chamber while the superheated stream enters the chamber. At the exit of each effect, three different streams are outlined. The saturated vapor exits the upper side of each effect and carries the needed thermal energy for the next stage of distillation, where its thermal energy level decreases successively through the stages and finally is uplifted to the primary energy level via an external power supply. The other two streams directing out from each effect are the freshwater stream (extracting out directly towards a water tank) and the brine stream, which is successively reinjected to the subsequent effect.

3. Materials and methods

Three sub-sections of wind turbine modeling, thermodynamic evaluation, and the expanded performance factors for the devised set-up are organized in this section.

3.1. Wind turbine modeling

Relations of the wind turbine modeling comprehensively are

presented in (Rostami et al., 2021) and excluded here to avoid unnecessary repetition.

The amount of thermal heat wasted in the gear box and generator of the wind turbine (\dot{Q}_{WH}) can be expressed as (Khalilzadeh and Hossein Nezhad, 2018):

$$\dot{Q}_{WH} = (1 - \eta_{gear})(1 - \eta_{gen})\dot{W}_{WT,avg} \quad (1)$$

where, η_{gen} and η_{gear} are the thermal waste efficiency of the generator and gearbox, respectively. As the selected wind turbine has no gearbox (direct driven), η_{gear} is assumed to be zero. The net wind turbine power can be written as follows:

$$\dot{W}_{net,WT} = \dot{W}_{avg,WT} - \dot{Q}_{WH} \quad (2)$$

In this study the Goldwind GW136/4800 model is assumed for the wind turbine. The main specifications of the GW-136 are listed in Table 1.

The wind speed at different heights varies remarkably. Therefore, the wind speed velocity at the desired altitude should be determined (Ehyaei et al., 2019):

$$u(z_2) = u(z_1) \left(\frac{z_2}{z_1} \right)^\epsilon \quad (3)$$

In which,

Table 1

Input design parameters for thermodynamic simulation of the devised WT/HDH-MED-MVC system.

Parameter	value	Ref.
Reference temperature, T_0 (K)	298.15	(Rostamzadeh and Rostami, 2020b)
Reference pressure, P_0 (bar)	1.01	(Rostamzadeh and Rostami, 2020b)
Reference salinity of seawater, S_0 (g.kg ⁻¹)	35	(Rostamzadeh and Rostami, 2020b)
Standard molar chemical exergy of water, \bar{x}_{ch}^0 (kJ/kmol)	45	(Ghiasirad et al., 2020)
Reference relative humidity, ϕ_0 (%)	65	(Rostami et al., 2021)
HDH unit		
Terminal temperature difference of heater, TTD_h (K)	10	(Rostamzadeh et al., 2018a)
Desalination top temperature, T_{13} (K)	333.15	(Abdollahi Haghghi et al., 2019)
Pump isentropic efficiency, $\eta_{is,pum}$ (%)	85	(Javanfam et al., 2022)
Humidifier effectiveness, ϵ_{Hum} (%)	85	(Ghiasirad et al., 2021a)
Dehumidifier effectiveness, ϵ_{DHum} (%)	85	(Ghiasirad et al., 2021a)
Desalination mass flowrate ratio, MR WT set-up	1.8	(Elbassoussi et al., 2021)
Terminal temperature difference of RHX, TTD_{RHX} (K)	2	(Rostami et al., 2021)
Reynolds number on tube side of RHX	2300	(Rostami et al., 2021)
Reynolds number on shell side of RHX	3500	(Rostami et al., 2021)
Average wind speed, u_{avg} (m.s ⁻¹)	9	Assumed
Cut-in wind speed, u_c (m.s ⁻¹)	2.5	(Rostamzadeh et al., 2021)
Rated wind speed, u_r (m.s ⁻¹)	11.2	(Rostamzadeh et al., 2021)
Furling wind speed, u_f (m.s ⁻¹)	26	(Rostamzadeh et al., 2021)
Swept area, A_s (m ²)	14526	(Rostamzadeh et al., 2021)
Maximum wind turbine output power, \dot{W}_m (kW)	4800	(Rostamzadeh et al., 2021)
Generator efficiency, η_{gen} (%)	93	(Rostamzadeh et al., 2021)
Reference height, z_1 (m)	10	(Rostamzadeh et al., 2021)
Tower height, z_2 (m)	86	(Rostamzadeh et al., 2021)
MED+MVC		
Compressor isentropic efficiency, $\eta_{is,comp}$ (%)	90	(Rostamzadeh et al., 2020)
Temperature difference between each effect, ΔT_{effect}	1.35	Assumed
Distilled water temperature of first effect, T_{17} (K)	334.15	(Razmi et al., 2019)
Pump isentropic efficiency, η_{pum}	0.9	(Rostamzadeh et al., 2018a)
BFR	0.9	Assumed

$$\epsilon = \alpha - \beta \log_{10} u(z_1) \quad (4)$$

Where z_2 and z_1 are the wind turbine and standard altitude (m), respectively. Also, $u(z_1)$ and $u(z_2)$ are the wind speed at these heights. α and β are constant coefficients and are assumed to be 0.11 and 0.061 during the day and 0.38 and 0.209 during the night (Ehyaei et al., 2019).

3.2. Thermodynamic evaluation

Some necessary assumptions and input data are needed to model a system properly, and the modeling would only be validated with them. In this subsection, researchers have all the required values collected in the following points and Table 1.

- All thermodynamic processes described by the governing equations are developed under steady-state conditions.
- The temperature of the purified water is set as the average temperature of air streams in the closed loop of the HDH unit (Ghiasirad et al., 2021a).
- The relative humidity of air in closed loop of the HDH unit is presumed to be 90% (Ghiasirad et al., 2021a).
- Physical and chemical exergies of streams associated with pure and saline water are calculated.
- Seawater enters the desalination unit at dead state temperature and pressure (Ghiasirad et al., 2021a)

Table 2

Mass, salinity, and energy balance equations for each component of the proposed minimal liquid discharge hybrid desalination system.

Component	Mass and salinity balances	Energy Balance
Wind Turbine	$\dot{m}_1 = \dot{m}_2$	$\dot{Q}_{WH} = \dot{m}_2(h_1 - h_2)$
RHX	$\dot{m}_3 = \dot{m}_5$	$\dot{Q}_{RHX} = \dot{m}_3(h_3 - h_5)$
Pump 1	$\dot{m}_4 = \dot{m}_5$	$\dot{W}_{pum1} = \dot{m}_4(h_5 - h_4)$ $\eta_{pum} = (h_{5,isen} - h_4)/(h_5 - h_4)$
Heater	$\dot{m}_{10} = \dot{m}_{11}$	$\epsilon_{Heater} = (T_3 - T_4)/(T_3 - T_{10})$ $T_4 = T_{10} + TTD_{Heater}$ $\dot{Q}_{heater} = \epsilon_{Heater} \dot{m}_3(h_3 - h_4)$
HDH System	$\dot{m}_8 = \dot{m}_9$ $X_8 = X_9 = X_0$ $\dot{m}_{12} = \dot{m}_{10} - \dot{m}_{13}$ $\dot{m}_{10} X_{10} = \dot{m}_{12} X_{12}$ $\dot{m}_{11} = \dot{m}_{10}$ $X_{11} = X_{10}$ $MR = \dot{m}_8/\dot{m}_{da}$ $\dot{m}_6 = \dot{m}_{da} * (1 + \omega_6)$ $\dot{m}_7 = \dot{m}_{da} * (1 + \omega_7)$ $\dot{m}_{13} = \dot{m}_{da} * (\omega_7 - \omega_6)$	$\dot{Q}_{heater} = \dot{m}_{10}(h_{11} - h_{10})$ $\begin{cases} \epsilon_{pht} = \max(yy, zz) \\ yy = (h_7 - h_6)/(h_7 - h_{6,ideal}) \\ zz = (h_9 - h_8)/(h_9,ideal - h_8) \end{cases}$ $\begin{cases} \epsilon_{Hum} = \max(pp, qq) \\ pp = (h_7 - h_6)/(h_7,ideal - h_6) \\ qq = (h_{11} - h_{12})/(h_{11} - h_{12,ideal}) \end{cases}$ $\dot{m}_{da}(h_7 - h_6) = \dot{m}_8(h_9 - h_8) + \dot{m}_{13}h_{13}$ $\dot{m}_{da}(h_7 - h_6) = \dot{m}_{11}h_{11} - \dot{m}_{12}h_{12}$
Effect 1	$\dot{m}_{14} = \dot{m}_{12}/N_{eff}$ $\dot{m}_{17} = \dot{m}_{45}$ $\dot{m}_{14} = \dot{m}_{15} + \dot{m}_{16}$ $\dot{m}_{14}X_{14} = \dot{m}_{16}X_{16}$	$T_{15} = T_{17} - \Delta T_{eff}$ $T_{16} = T_{15}$ $\dot{Q}_{eff1} = \dot{m}_{16}h_{16} + \dot{m}_{15}h_{15} - \dot{m}_{14}h_{14}$ $\dot{Q}_{eff1} = \dot{m}_{45}(h_{45} - h_{17})$
Effect 2	$\dot{m}_{18} = \dot{m}_{12}/N_{eff}$ $\dot{m}_{21} = \dot{m}_{15}$ $\dot{m}_{18} + \dot{m}_{16} = \dot{m}_{19} + \dot{m}_{20}$ $\dot{m}_{18}X_{18} + \dot{m}_{16}X_{16} = \dot{m}_{20}X_{20}$	$T_{19} = T_{15} - \Delta T_{eff}$ $T_{19} = T_{b20}$ $\dot{Q}_{eff2} = \dot{m}_{19}h_{19} + \dot{m}_{20}h_{20} - \dot{m}_{18}h_{18} - \dot{m}_{16}h_{16}$ $\dot{Q}_{eff2} = \dot{m}_{15}(h_{15} - h_{21})$
Effect 3	$\dot{m}_{22} = \dot{m}_{12}/N_{eff}$ $\dot{m}_{19} = \dot{m}_{25}$ $\dot{m}_{20} + \dot{m}_{22} = \dot{m}_{23} + \dot{m}_{24}$ $\dot{m}_{20}X_{20} + \dot{m}_{22}X_{22} = \dot{m}_{24}X_{24}$	$T_{23} = T_{19} - \Delta T_{eff}$ $T_{23} = T_{24}$ $\dot{Q}_{eff3} = \dot{m}_{23}h_{23} + \dot{m}_{24}h_{24} - \dot{m}_{22}h_{22} - \dot{m}_{20}h_{20}$ $\dot{Q}_{eff3} = \dot{m}_{19}(h_{19} - h_{25})$
Effect 4	$\dot{m}_{26} = \dot{m}_{12}/N_{eff}$ $\dot{m}_{23} = \dot{m}_{29}$ $\dot{m}_{24} + \dot{m}_{26} = \dot{m}_{27} + \dot{m}_{28}$ $\dot{m}_{24}X_{24} + \dot{m}_{26}X_{26} = \dot{m}_{28}X_{28}$	$T_{27} = T_{23} - \Delta T_{eff}$ $T_{27} = T_{28}$ $\dot{Q}_{eff4} = \dot{m}_{27}h_{27} + \dot{m}_{28}h_{28} - \dot{m}_{26}h_{26} - \dot{m}_{24}h_{24}$ $\dot{Q}_{eff4} = \dot{m}_{23}(h_{23} - h_{29})$
Effect 5	$\dot{m}_{30} = \dot{m}_{12}/N_{eff}$ $\dot{m}_{27} = \dot{m}_{33}$ $\dot{m}_{28} + \dot{m}_{30} = \dot{m}_{31} + \dot{m}_{32}$ $\dot{m}_{28}X_{28} + \dot{m}_{30}X_{30} = \dot{m}_{32}X_{32}$	$T_{31} = T_{27} - \Delta T_{eff}$ $T_{31} = T_{32}$ $\dot{Q}_{eff5} = \dot{m}_{31}h_{31} + \dot{m}_{32}h_{32} - \dot{m}_{30}h_{30} - \dot{m}_{28}h_{28}$ $\dot{Q}_{eff5} = \dot{m}_{27}(h_{27} - h_{33})$
Effect 6	$\dot{m}_{34} = \dot{m}_{12}/N_{eff}$ $\dot{m}_{31} = \dot{m}_{37}$ $\dot{m}_{32} + \dot{m}_{34} = \dot{m}_{35} + \dot{m}_{36}$ $\dot{m}_{32}X_{32} + \dot{m}_{34}X_{34} = \dot{m}_{36}X_{36}$	$T_{35} = T_{31} - \Delta T_{eff}$ $T_{35} = T_{36}$ $\dot{Q}_{eff6} = \dot{m}_{35}h_{35} + \dot{m}_{36}h_{36} - \dot{m}_{34}h_{34} - \dot{m}_{32}h_{32}$ $\dot{Q}_{eff6} = \dot{m}_{31}(h_{31} - h_{37})$
Effect 7	$\dot{m}_{38} = \dot{m}_{12}/N_{eff}$ $\dot{m}_{35} = \dot{m}_{41}$ $\dot{m}_{36} + \dot{m}_{38} = \dot{m}_{39} + \dot{m}_{40}$ $\dot{m}_{36}X_{36} + \dot{m}_{38}X_{38} = \dot{m}_{40}X_{40}$	$T_{39} = T_{35} - \Delta T_{eff}$ $T_{39} = T_{40}$ $\dot{Q}_{eff7} = \dot{m}_{39}h_{39} + \dot{m}_{40}h_{40} - \dot{m}_{38}h_{38} - \dot{m}_{36}h_{36}$ $\dot{Q}_{eff7} = \dot{m}_{35}(h_{35} - h_{41})$
MVC	$\dot{m}_{45} = \dot{m}_{39}$	$\eta_{MVC} = (h_{45,isen} - h_{39})/(h_{45} - h_{39})$ $\dot{W}_{MVC} = \dot{m}_{45}(h_{45} - h_{39})$
Mix 3	$\dot{m}_{42} = \dot{m}_{17} + \dot{m}_{21} + \dot{m}_{25} + \dot{m}_{29} + \dot{m}_{33} + \dot{m}_{37} + \dot{m}_{41}$	$\dot{m}_{42} * h_{42} = \dot{m}_{17} * h_{17} + \dot{m}_{21} * h_{21} + \dot{m}_{25} * h_{25} + \dot{m}_{29} * h_{29} + \dot{m}_{33} * h_{33} + \dot{m}_{37} * h_{37} + \dot{m}_{41} * h_{41}$
Pump 2	$\dot{m}_{43} = \dot{m}_{42}$	$\eta_{pum2} = (h_{43,isen} - h_{42})/(h_{43} - h_{42})$ $\dot{W}_{pum2} = \dot{m}_{43}(h_{43} - h_{42})$
Mix 1	$\dot{m}_{10} = \dot{m}_9 + \dot{m}_{46}$ $\dot{m}_{10}X_{10} = \dot{m}_9X_9 + \dot{m}_{46}X_{46}$	$\dot{m}_{10}h_{10} = \dot{m}_9h_9 + \dot{m}_{46}h_{46}$

(continued on next page)

Table 2 (continued)

Component	Mass and salinity balances	Energy Balance
Mix 2	$\dot{m}_{44} = \dot{m}_{13} + \dot{m}_{43}$	$\dot{m}_{44}h_{44} = \dot{m}_{13}h_{13} + \dot{m}_{43}h_{43}$
Rejection	$\dot{m}_{46} = BFR * \dot{m}_{40}$	$h_{47} = h_{46} = h_{40}$
brine Split	$\dot{m}_{47} = \dot{m}_{40} - \dot{m}_{46}$	
	$sal_{47} = sal_{46} = sal_{40}$	

Table 3

Equations derived for exergy of fuel, product, and loss for each component.

Components	Exergy Equations	$\dot{Ex}_{Pr,k}$	$\dot{Ex}_{L,k}$
Wind turbine	$\dot{Ex}_{wind,in} - \dot{Ex}_{wind,out}$	$\dot{W}_{WT} - \dot{Q}_{waste} + \dot{Ex}_1 - \dot{Ex}_2$	-
RHX	$\dot{Ex}_1 - \dot{Ex}_2$	$\dot{Ex}_3 - \dot{Ex}_5$	-
Pump 1	\dot{W}_{pump1}	$\dot{Ex}_5 - \dot{Ex}_4$	-
Heater	$\dot{Ex}_3 - \dot{Ex}_4$	$\dot{Ex}_{11} - \dot{Ex}_{10}$	-
Dehumidifier	$\dot{Ex}_7 - \dot{Ex}_6$	$\dot{Ex}_9 - \dot{Ex}_8 + \dot{Ex}_{13}$	-
Humidifier	$\dot{Ex}_{11} - \dot{Ex}_{12}$	$\dot{Ex}_7 - \dot{Ex}_6$	-
MVC	\dot{W}_{MVC}	$\dot{Ex}_{45} - \dot{Ex}_{39}$	-
Effect I	$\dot{Ex}_{45} - \dot{Ex}_{17}$	$\dot{Ex}_{15} + \dot{Ex}_{16} - \dot{Ex}_{14}$	-
Effect II	$\dot{Ex}_{15} - \dot{Ex}_{21}$	$\dot{Ex}_{19} + \dot{Ex}_{20} - \dot{Ex}_{16} - \dot{Ex}_{18}$	-
Effect III	$\dot{Ex}_{19} - \dot{Ex}_{25}$	$\dot{Ex}_{23} + \dot{Ex}_{24} - \dot{Ex}_{22} - \dot{Ex}_{20}$	-
Effect IV	$\dot{Ex}_{23} - \dot{Ex}_{29}$	$\dot{Ex}_{27} + \dot{Ex}_{28} - \dot{Ex}_{26} - \dot{Ex}_{24}$	-
Effect V	$\dot{Ex}_{27} - \dot{Ex}_{33}$	$\dot{Ex}_{31} + \dot{Ex}_{32} - \dot{Ex}_{30} - \dot{Ex}_{28}$	-
Effect VI	$\dot{Ex}_{31} - \dot{Ex}_{37}$	$\dot{Ex}_{35} + \dot{Ex}_{36} - \dot{Ex}_{34} - \dot{Ex}_{32}$	-
Effect VII	$\dot{Ex}_{35} - \dot{Ex}_{41}$	$\dot{Ex}_{39} + \dot{Ex}_{46} - \dot{Ex}_{38} - \dot{Ex}_{36}$	\dot{Ex}_{47}
Pump 2	\dot{W}_{pump2}	$\dot{Ex}_{43} - \dot{Ex}_{42}$	-
Mix 1	$\dot{Ex}_9 + \dot{Ex}_{46}$	\dot{Ex}_{10}	-
Mix 2	$\dot{Ex}_{43} + \dot{Ex}_{13}$	\dot{Ex}_{44}	-
Mix 2	$\dot{Ex}_{17} + \dot{Ex}_{21} + \dot{Ex}_{25} + \dot{Ex}_{29} + \dot{Ex}_{33} + \dot{Ex}_{37} + \dot{Ex}_{41}$	\dot{Ex}_{42}	-

- All processes inside the devised hybrid desalination unit operate under atmospheric pressure (Rostamzadeh et al., 2020).
- Pumps and MVC are modelled using isentropic efficiencies.
- Distilled water and steam streams flowing inside the MED-MVC unit are saturated (Rostamzadeh et al., 2020)
- Outlet brine and steam of each effect have the same temperatures (Rostamzadeh et al., 2020).
- Since the boiling point elevation (BPE) for a stream with salinity <100 g/kg and $T < 52^\circ\text{C}$ is lower than 1°C (Elsayed et al., 2021). Thus, the BPE is negligible.

3.2.1. Energy analysis

Conservation equations consisting of mass, energy, and salinity quantities can be expressed respectively as (Bejan and Tsatsaronis, 1996):

Mass balance Eq.:

$$\sum \dot{m}_{in} - \sum \dot{m}_{out} = 0 \tag{5}$$

Energy balance Eq.:

Table 4

Model comparison between the reference system and devised WT/HDH-MED-MVC system.

Systems	SWC ($\frac{kW}{m^3}$)	$\dot{m}_{FW}(\frac{m^3}{h})$	$\dot{W}_{net}(kW)$	$\eta_{ex,tot}(\%)$
<i>Wind speed = 8 $\frac{m}{s}$</i>				
WT/HDH-RO	26.96	2.402	2376	30.98
WT/HDH-MED-MVC (4 effects)	42.07	1.527	2375	30.99
WT/HDH-MED-MVC (5 effects)	30.81	2.15	2373	30.98
WT/HDH-MED-MVC (6 effects)	26.38	2.564	2372	30.97
WT/HDH-MED-MVC (7 effects)	23.94	2.871	2371	30.97
<i>Wind speed = 9 $\frac{m}{s}$</i>				
WT/HDH-RO	24.5	3.604	3221	31.51
WT/HDH-MED-MVC (4 effects)	38.7	2.265	3220	31.52
WT/HDH-MED-MVC (5 effects)	28.4	3.192	3217	31.51
WT/HDH-MED-MVC (6 effects)	24.33	3.811	3215	31.5
WT/HDH-MED-MVC (7 effects)	22.09	4.271	3213	31.5
<i>Wind speed = 10 $\frac{m}{s}$</i>				
WT/HDH-RO	22.72	5.273	4343	32.68
WT/HDH-MED-MVC (4 effects)	36.23	3.281	4343	32.7
WT/HDH-MED-MVC (5 effects)	26.62	4.629	4339	32.69
WT/HDH-MED-MVC (6 effects)	22.83	5.532	4336	32.68
WT/HDH-MED-MVC (7 effects)	20.74	6.205	4333	32.67
<i>Wind speed = 11 $\frac{m}{s}$</i>				
WT/HDH-RO	22.59	5.439	4453	26.31
WT/HDH-MED-MVC (4 effects)	36.06	3.382	4453	26.33
WT/HDH-MED-MVC (5 effects)	26.49	4.772	4448	26.32
WT/HDH-MED-MVC (6 effects)	22.72	5.702	4445	26.32
WT/HDH-MED-MVC (7 effects)	20.64	6.397	4443	26.31
<i>Wind speed = 12 $\frac{m}{s}$</i>				
WT/HDH-RO	22.59	5.439	4453	21.04
WT/HDH-MED-MVC (4 effects)	36.06	3.382	4453	21.05
WT/HDH-MED-MVC (5 effects)	26.49	4.772	4448	21.05
WT/HDH-MED-MVC (6 effects)	22.72	5.702	4445	21.04
WT/HDH-MED-MVC (7 effects)	20.64	6.397	4443	21.04

Input data for RO unit:

Element area =35.4 m²; Fouling factor = 0.85; Number of elements =7; Number of pressure vessels = 42; Recovery ratio = 0.3; Salt rejection percentage = 1.

$$\dot{Q}_{c.v.} - \dot{W}_{c.v.} = \sum (\dot{m}h)_{out} - \sum (\dot{m}h)_{in} \tag{6}$$

Salinity balance Eq.:

$$\sum (\dot{m}S)_{in} - \sum (\dot{m}S)_{out} = 0 \tag{7}$$

Desalination flow ratio (MR) of the HDH unit is expressed as follow:

$$MR = \frac{\dot{m}_{sw}}{\dot{m}_{da}} \tag{8}$$

Effectiveness of humidifier/dehumidifier (ϵ) is expressed as follows:

$$\epsilon = \frac{\Delta \dot{H}}{\Delta \dot{H}_{max}} \tag{9}$$

The component-based mass, energy, and salinity relations for each element of the proposed hybrid desalination system are listed in Table 2.

3.2.2. Exergy analysis

Concerning the second law of thermodynamics, the exergy balance equation for each component is articulated in terms of the exergy rates of all streams exiting and entering the kth component as below(Bejan and Tsatsaronis, 1996):

$$\dot{Ex}_{D,k} = \sum_{i=1}^k \dot{Ex}_{in,i} - \sum_{i=1}^k \dot{Ex}_{out,i} \tag{10}$$

or, in terms of exergy rate of product (\dot{Ex}_{Pr}), exergy rate of fuel (\dot{Ex}_{Fu}), exergy rate of loss ($\dot{Ex}_{L,k}$), and exergy rate of destruction ($\dot{Ex}_{D,k}$), Eq. (10)

Table 5
Main thermodynamic properties evaluated for each state of the devised WT/HDH-MED-MVC system.

State	Fluid	T (K)	P (bar)	h ($\frac{kJ}{kg}$)	s ($\frac{kJ}{kg K}$)	\dot{m} ($\frac{kg}{s}$)	$\dot{E}x$ (kW)
1	Water	375.1	9.29	428	1.329	1.557	60.66
2	Water	337.9	9.29	272	0.8904	1.557	21.05
3	Water	371	9.115	410.5	1.282	1.653	58.6
4	Water	335.9	1.013	262.6	0.8652	1.653	19.35
5	Water	335.9	9.115	263.6	0.8656	1.653	20.74
6	Air	316.9	1.013	183	6.224	0.978	3.102
7	Air	333.5	1.013	417.2	6.95	1.055	22.21
8	Brine	298.2	1.013	99.77	0.3498	1.67	0
9	Brine	328.2	1.013	220.1	0.7345	1.67	9.452
10	Brine	325.9	1.013	196.8	0.6396	6.853	45.88
11	Brine	333.2	1.013	224.6	0.7238	6.853	64.11
12	Brine	325.5	1.013	195.1	0.6336	6.776	44.98
13	Freshwater	324	1.013	213.1	0.7152	0.07663	0.5262
14	Brine	325.5	1.013	195.1	0.6336	0.968	6.426
15	Steam	332.9	0.1967	2608	7.913	0.1508	38.63
16	Brine	332.9	1.013	218.4	0.6947	0.8172	8.638
17	Freshwater	334.2	0.2089	255.4	0.8438	0.1586	1.719
18	Brine	325.5	1.013	195.1	0.6336	0.968	6.426
19	Steam	331.6	0.1852	2606	7.934	0.1428	35.36
20	Brine	331.6	1.013	213.6	0.6808	1.642	16.46
21	Freshwater	332.9	0.1967	249.9	0.8275	0.1508	1.547
22	Brine	325.5	1.013	195.1	0.6336	0.968	6.426
23	Steam	330.3	0.1742	2604	7.955	0.1385	33.1
24	Brine	330.3	1.013	208.9	0.6666	2.472	23.5
25	Freshwater	331.6	0.1852	244.5	0.8112	0.1428	1.385
26	Brine	325.5	1.013	195.1	0.6336	0.968	6.426
27	Steam	329	0.1638	2601	7.977	0.138	31.78
28	Brine	329	1.013	204	0.6521	3.302	29.79
29	Freshwater	330.3	0.1742	239	0.7947	0.1385	1.269
30	Brine	325.5	1.013	195.1	0.6336	0.968	6.426
31	Steam	327.7	0.1539	2599	7.998	0.1411	31.28
32	Brine	327.7	1.013	199.2	0.6373	4.129	35.38
33	Freshwater	329	0.1638	233.6	0.7782	0.138	1.192
34	Brine	325.5	1.013	195.1	0.6336	0.968	6.426
35	Steam	326.4	0.1445	2597	8.02	0.148	31.51
36	Brine	326.4	1.013	194.3	0.6223	4.949	40.31
37	Freshwater	327.7	0.1539	228.2	0.7617	0.1411	1.149
38	Brine	325.5	1.013	195.1	0.6336	0.968	6.426
39	Steam	325.1	0.1357	2595	8.042	0.1586	32.35
40	Brine	325.1	1.013	189.3	0.6069	5.758	44.65
41	Freshwater	326.4	0.1445	222.7	0.745	0.148	1.134
42	Freshwater	330.3	0.1748	239.3	0.7956	1.018	9.353
43	Freshwater	330.3	1.013	239.4	0.7957	1.018	9.441
44	Freshwater	329.9	1.013	237.6	0.7901	1.095	9.956
45	Steam	364.9	0.2089	2670	8.063	0.1586	43.35
46	Brine	325.1	1.013	189.3	0.6069	5.182	40.19
47	Brine	325.1	1.013	189.3	0.6069	0.5758	4.465

can be re-written as (Bejan and Tsatsaronis, 1996):

$$\dot{E}x_{Fu,k} = \dot{E}x_{Pr,k} + \dot{E}x_{D,k} + \dot{E}x_{L,k} \quad (11)$$

The overall exergy rate for the k th component is articulated as follow (Bejan and Tsatsaronis, 1996):

$$\dot{E}x_k = \dot{E}x_{ph,k} + \dot{E}x_{ch,k} \quad (12)$$

where,

$$\dot{E}x_{ph,k} = \dot{m}(h - h_0 - T_0(s - s_0))_k \quad (13)$$

It is worth mentioning that the whole modelling and seawater's physical and chemical exergy components have been calculated via the EES library by defining a module-based predefined function (Nayar et al., 2016). However, the chemical exergy of steam and water can be found using the following equation:

$$\dot{E}x_{ch,H_2O,k} = \dot{m} \left(\frac{e x_{ch,H_2O}^0}{M_{H_2O}} \right)_k \quad (14)$$

In which, $e x_{ch,H_2O}^0$ is the standard chemical exergy of water assumed

to be 45 (kJ/kmol.K) (Ghiasirad et al., 2020)

Additionally, the chemical exergy of the humid air is reported in Ref. (Ghiasirad et al., 2021b)

Regarding the moist air, its specific exergy is expressed as (Wepfer et al., 1979):

$$e x_{da} = (c_{p,a} + \omega c_{p,v}) T_0 \left(\frac{T}{T_0} - 1 - \ln \frac{T}{T_0} \right) + (1 + 1.608\omega) R_a T_0 \ln \frac{P}{P_0} + R_a T_0 \left[(1 + 1.608\omega) \ln \frac{1 + 1.608\omega_0}{1 + 1.608\omega} + 1.608\omega \ln \frac{\omega}{\omega_0} \right] \quad (15)$$

where,

$$\omega = \frac{\dot{m}_v}{\dot{m}_a} \quad (16)$$

In Eq. (15) the temperature and pressure of air at the outlet and inlet streams of the wind turbine are differing with velocity as follows:

$$T = 35.74 + 0.6215 \times T_{air} - 35.75 \times u^{0.16} + 0.4274 \times T_{air} \times u^{0.16} \quad (17)$$

In Eq. (17), the unit of T_{air} is °F (T (°F) = $\frac{9}{5} T$ (°C) + 32).

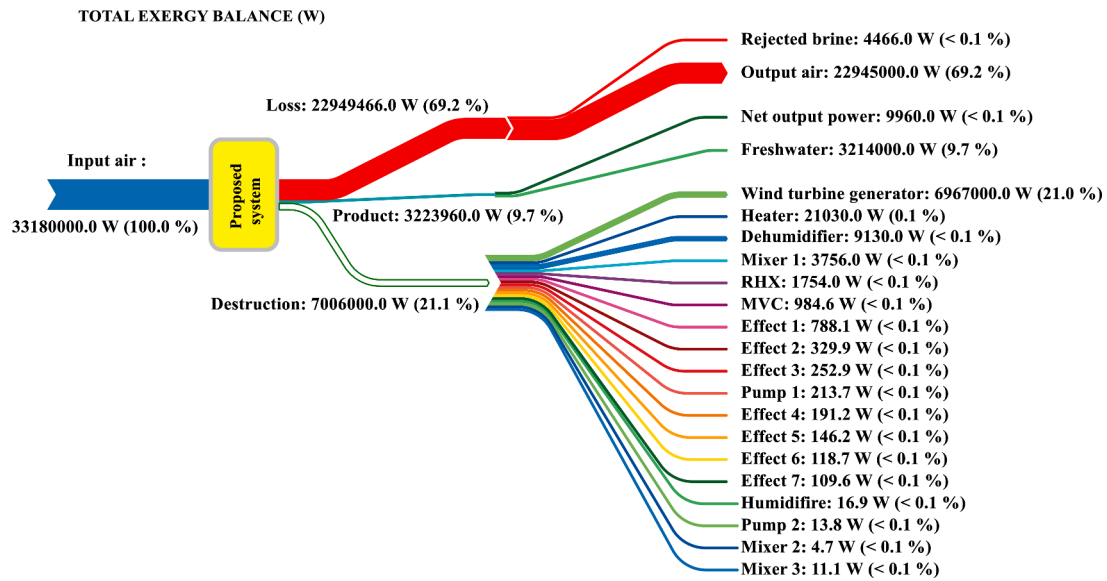


Fig. 3. Grossmann exergy flow diagram for the WT-HDH-MED-MVC system.

$$P = P_0 \pm \frac{u^2}{2} \quad (18)$$

The generic term for the exergy efficiency can be expressed as:

$$\eta_{ex,k} = \frac{\dot{E}x_{out}}{\dot{E}x_{in}} = \frac{\dot{E}x_{Pr,k}}{\dot{E}x_{Fu,k}} \quad (19)$$

All exergy relations required for each component of the proposed hybrid desalination system are derived and displayed in Table 3.

3.3. Performance criteria

Total energy efficiency of the devised system is articulated as:

$$\eta_{en,tot} = \frac{\dot{W}_{net} + \dot{m}_{21} \times h_{fg,21}}{\dot{E}n_{wind, in} - \dot{E}n_{wind, out}} \quad (20)$$

where, \dot{W}_{net} , $\dot{E}n_{wind, in}$, and $\dot{E}n_{wind, out}$ are the net electricity, rate of the input and output energy of the wind and can be expressed respectively as follows:

$$\dot{W}_{net} = \dot{W}_{avg,WT} - \dot{Q}_{WH} - \dot{W}_{pum1} - \dot{W}_{pum2} - \dot{W}_{MVC} \quad (21)$$

$$\dot{E}n_{wind, in} = \rho A_s u_{@z_2} \left(\frac{1}{2} u_{@z_2}^2 + h_{in} \right) \quad (22)$$

$$\dot{E}n_{wind, out} = \rho A_s u_{@z_2} \left(\frac{1}{2} \left(\frac{u_{@z_2}}{3} \right)^2 + h_{out} \right) \quad (23)$$

The total exergy efficiency of the proposed system is expressed as:

$$\eta_{ex,tot} = \frac{\dot{W}_{net} + \dot{E}x_{21}}{\dot{E}x_{wind, in} - \dot{E}x_{wind, out}} \quad (24)$$

Other essential metrics for the proposed hybrid desalination system are the specific work consumption (SWC) and performance ratio (PR), which are presented in Eq. (25) and (26) respectively as:

$$SWC = \frac{\dot{W}_{pum2} + \dot{W}_{MVC} + \frac{1}{3} \dot{Q}_{WH}}{\dot{m}_{21} @ (m^2/h)} \quad (25)$$

$$PR = \frac{\dot{m}_{21} \times h_{fg,21}}{\dot{Q}_{WH} + \dot{W}_{pum1} + \dot{W}_{pum2} + \dot{W}_{MVC}} \quad (26)$$

4. Model verification and comparison

This part consists of two sub-sections: Model verification and model comparison. In the first part, the accuracy of the results has been examined with previously published data. In the second sub-section, the performance of the present model is compared with those of the HDH-RO system, as proposed by Rostamzadeh et al. (Rostamzadeh et al., 2021) to demonstrate the superiorities and practicalities of the newly devised model.

4.1. Model verification

Because the new set-up consists of three main subsystems of an HDH unit, a waste heat recovery sub-unit of the wind turbine, and a MED-MVC unit, it is highly indispensable to verify the developed mathematical codes with accessible, valuable works. Since the authors have used identical subsystems in the previous results for different purposes, the same developed codes verified in our previous works (Rostamzadeh, 2021; Rostamzadeh et al., 2020), and (Rostami et al., 2021) are used here for these subsystems. Hence, any explanation about the verification processes is excluded here for brevity.

4.2. Model comparison

In this sub-section, a comparison between the WT/HDH-RO system (shown in Fig. 1) and the devised WT/HDH-MED-MVC systems with a different number of effects are carried out, and the results are illustrated in Table 4. To find an efficient system, four numbers of effects for the MED-MVC unit are considered. The configurations include MED-MVC systems with four, five, six, and seven effects. To achieve an impartial comparison between the reference system and the new HDH-MED-MVC units, the input data of the wind turbine and the HDH unit is the same for all cases as reported in Table 1. Accordingly, the humidifier and dehumidifier effectiveness, HDH top temperature, HDH mass flow ratio ($\frac{\dot{m}_{s}}{\dot{m}_{dry air}}$), and input salinity concentration are fixed at 0.8, 0.8, 333.15 K, 1.8, and 35 g/kg, respectively. Since the reference system includes an RO unit, there are some specific input data needed for modeling the RO unit. The required data for the RO unit is presented at the bottom of Table 4.

Table 4 illustrates the freshwater rate, SWC, net power, and exergy efficiency results in five different wind speeds for the reference system

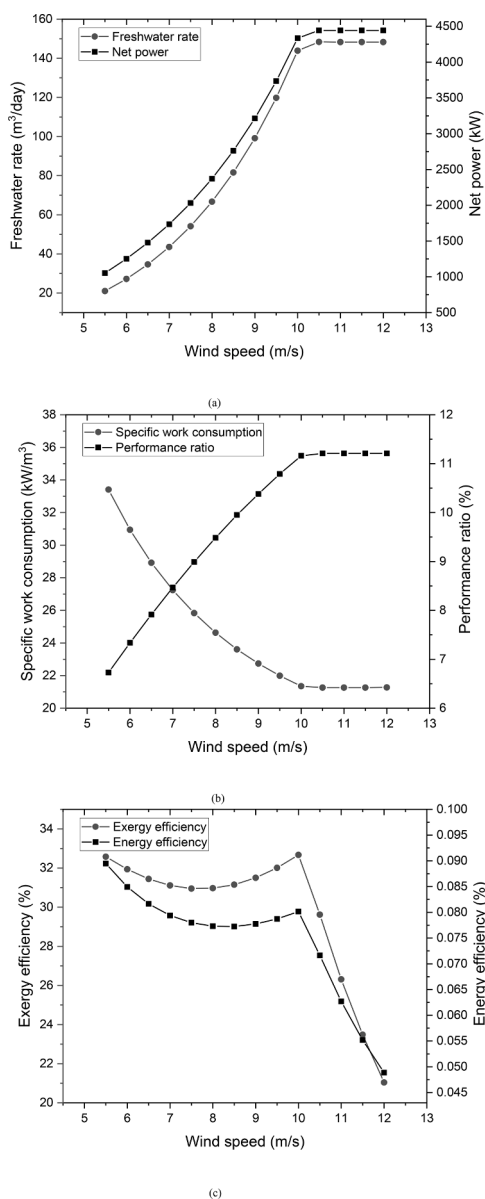


Fig. 4. Impact of wind speed on the: (a) freshwater rate and net power, (b) specific work consumption and performance ratio, and (c) exergy efficiency and energy efficiency.

and four different configurations of the WT-HDH-MED-MVC system. In terms of the amount of freshwater, increasing the number of effects increases the amount of freshwater. In the five different wind speeds, the amount of freshwater rate produced by the reference system is less than that produced by the MED-MVC unit with numbers of effects larger than six. According to the SWC, it is shown that with the rise in the number of effects, the SWC decreases significantly. In low speeds (e.g., lower than 10 m/s), the SWC of the MED-MVC unit with number of effects less than six is higher than the value seen in the reference system. While at high speeds (equal to or higher than 10 m/s), only the SWC of the MED-MVC unit with seven numbers of effects is less than that of the reference system. In general, the exergy efficiency and net power are increased with the rise of the wind speed in all devised new desalination systems. However, no significant difference between the exergy efficiency of different systems is seen at the same wind speeds.

5. Results and discussions

This section is organized into two sub-division of basic results and parametric assessment. Each sub-division is comprehensively described herein.

5.1. Basic results

For a base form of investigation, the thermodynamic properties of each point are presented in Table 5. These properties involve temperature, pressure, enthalpy, entropy, mass flow rate, and exergy rate.

Fig. 3 displays the exergy flow diagram for the WT-HDH-MED-MVC system for a wind speed of 9 m/s, humidifier, and dehumidifier effectiveness of 0.85, and temperature difference between each effect of 1.3. This figure demonstrates the share of each element to the total input exergy. Rejected brine and output air contribute 69.2% of the total exergy, while the share of destruction through the plant operation is 21.1%. The wind turbine has the highest exergy destruction of 6,967,000 W (21% of total input exergy), followed by the heater (21,030 W), similar to what is presented in (Rostamzadeh and Rostami, 2020b). As the figure depicts, the total exergy of products, which consists of net output power and freshwater exergy rate, possesses 9.7% of the total input exergy. In the proposed cycle, it is possible to lessen the exergy destructions by designing the cycle in hot and humid climates, decreasing the effectiveness of humidifier and dehumidifier, reducing the wind speed, 100% recycling of the brine, diminishing the temperature difference between MED effects.

5.2. Parametric assessment

The model comparison sub-section discussed the superiorities and inferiorities of different systems. As concluded, WT/HDH-MED-MVC unit with seven effects has the best performance among all devised systems. In this part, a parametric study is carried out to detect how the performance of the WT/HDH-MED-MVC unit with seven numbers of effects can be improved or deteriorated by re-adjusting the assumed input data. The impacts of the wind speed, HDH mass flow ratio, humidifier, and dehumidifier effectiveness on the main influenced performance criteria are investigated to achieve this goal. The primary objectives are the freshwater rate, net power, SWC, PR, exergy, and energy efficiencies.

5.2.1. Impact of wind speed

Fig. 4 depicts a variation of the freshwater rate, net power, SWC, PR, and exergy and energy efficiencies versus the wind speed. As Fig. 4(a) illustrates, with the rise of the wind speed, the freshwater rate is increased since increasing the wind speed increases the rotational speed of the wind turbine, which in turn can produce more dissipating heat. Similar to the freshwater rate, the net power as well as PR are increased with the increase of wind speed while the SWC is decreased. Since the value of the rated wind speed of the selected wind turbine is 11.2 m/s (it is equivalent to 10.08 m/s at the height of 10 m), the amounts of freshwater rate, net power, and performance ratio reach a maximum of 148.3 m³/day, 4443 kW, and 11.21% respectively, while the SWC reaches to its minimum value of 21.26 kW/m³. Fig. 4(c) displays the exergy and energy efficiency values versus wind speed. Three different regions are observed in this figure: (i) at wind speeds 5–8 m/s, the amount of exergy and energy efficiencies are decreased with the increase of wind speed, (ii) at wind speeds 8–10 m/s, the values of exergy and energy efficiencies are increased until the point where the wind speed reaches to the rated wind speed, and (iii) at wind speeds higher than 10 m/s the trend shows a sharp decline in exergy and energy efficiencies with the rise of wind speed. Having said that all the objectives shown in Fig. 4 follow a similar trend reported in Ref. (Rostamzadeh et al., 2021).

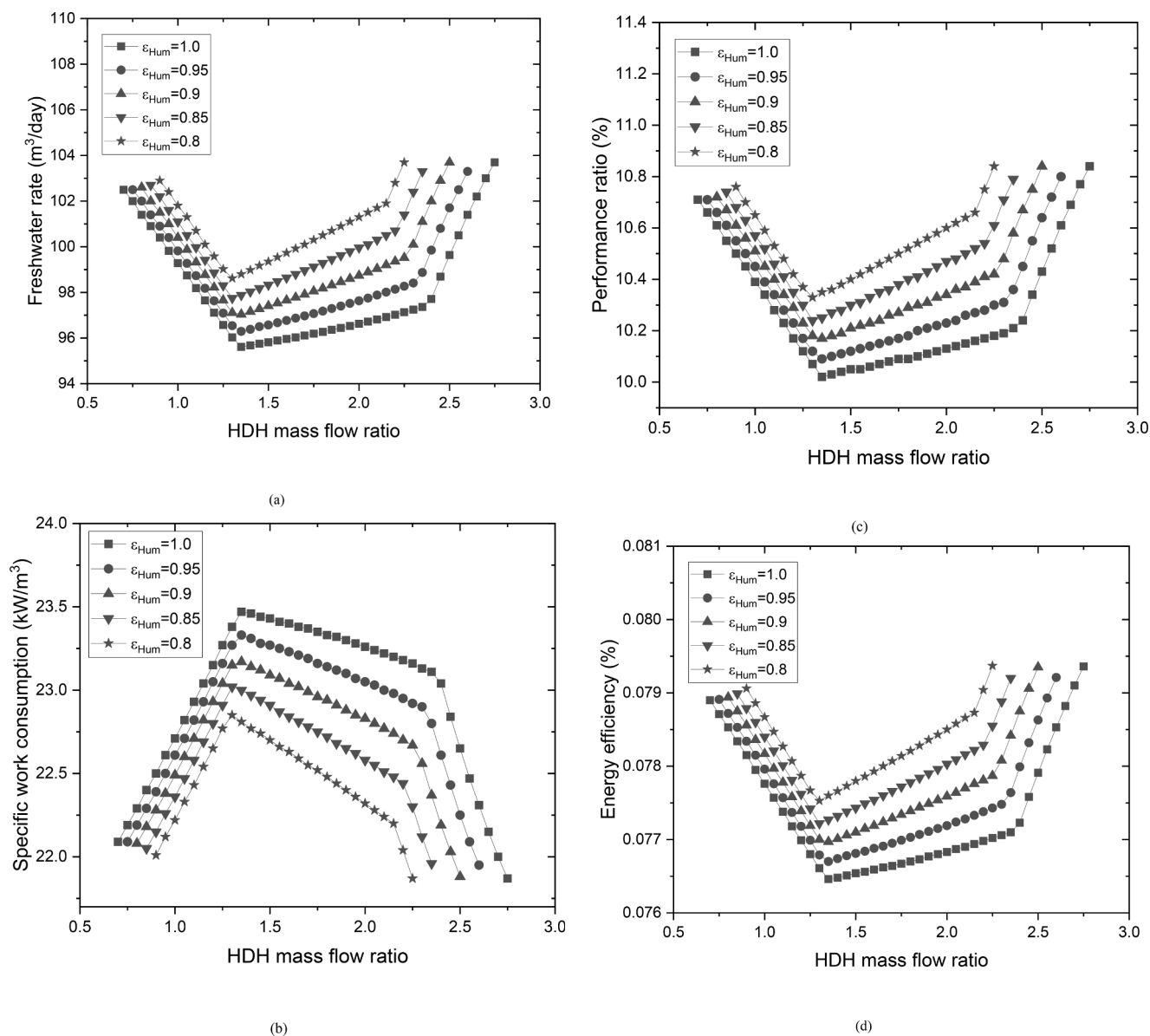


Fig. 5. Impact of HDH mass flow ratio on the: (a) freshwater rate, (b) specific work consumption, (c) performance ratio, (e) energy efficiency at different humidifier effectiveness levels. Square, circle, upward triangle, downward triangle, and star symbols represent value of dehumidifier effectiveness 1.0, 0.95, 0.9, 0.85 and 0.8, respectively, while the value of the dehumidifier effectiveness is set at 0.85.

5.2.2. Impact of the HDH mass flow ratio on the system

Fig. 5 presents the variation of freshwater rate, SWC, performance ratio, and energy efficiency versus the HDH mass flow ratio at five different values of humidifier effectiveness levels. In the figure, square, circle, upward triangle, downward triangle, and star symbols represent the values of the related performance metrics at different humidifier effectiveness of 1.0, 0.95, 0.9, 0.85, and 0.8, respectively. Illustrating the net power and exergy efficiency alteration trend is ignored here because of their tiny variation with the HDH mass flow ratio. It is important to note that for a detailed study of the effect of humidifier effectiveness, the value of dehumidifier effectiveness is fixed at 0.85. Fig. 5 shows that there are three different regions on the graphs. Accordingly, the freshwater rate, performance ratio, and energy efficiency decrease with the rise of HDH mass flow ratio in the range of 0.5–1.45. Although the freshwater rate, the performance ratio, and energy efficiency reached their minimum value for each humidifier's effectiveness at different HDH mass flow ratios, they all changed around 1.45 to 1.5. The freshwater rate, the performance ratio, and energy

efficiency increase with increasing the HDH mass flow ratio until their maximum value of 103.7 m³/day, 10.84%, 0.07937% for humidifier effectiveness of 0.8, 103.3 m³/day, 10.79%, 0.0792% for humidifier effectiveness of 0.85, 103.7 m³/day, 10.84%, 0.07935% for humidifier effectiveness of 0.9, 103.3 m³/day, 10.80%, 0.07921% for humidifier effectiveness of 0.95, and 103.7 m³/day, 10.84%, 0.07936% for humidifier effectiveness of 1.0, respectively. As shown in Fig. 5(a), the maximum value of the HDH mass flow ratio is different for each humidifier effectiveness. That is to say, the maximum HDH mass flow ratio for humidifier's effectiveness of 1.0, 0.95, 0.9, 0.85, and 0.8 is 2.75, 2.6, 2.5, and 2.25, respectively.

Unlike reported in previous studies investigating the effect of the humidifier effectiveness and HDH mass ratio on the freshwater capacity of a solo-HDH cycle (Narayan et al., 2010; Rostamzadeh et al., 2021, 2018b; Rostamzadeh and Rostami, 2020b), the results of the present study show that there is minimal freshwater rate, performance ratio, and energy efficiency (at a constant HDH mass flow ratio) versus varying the humidifier effectiveness. This can be attributed to directing the highly

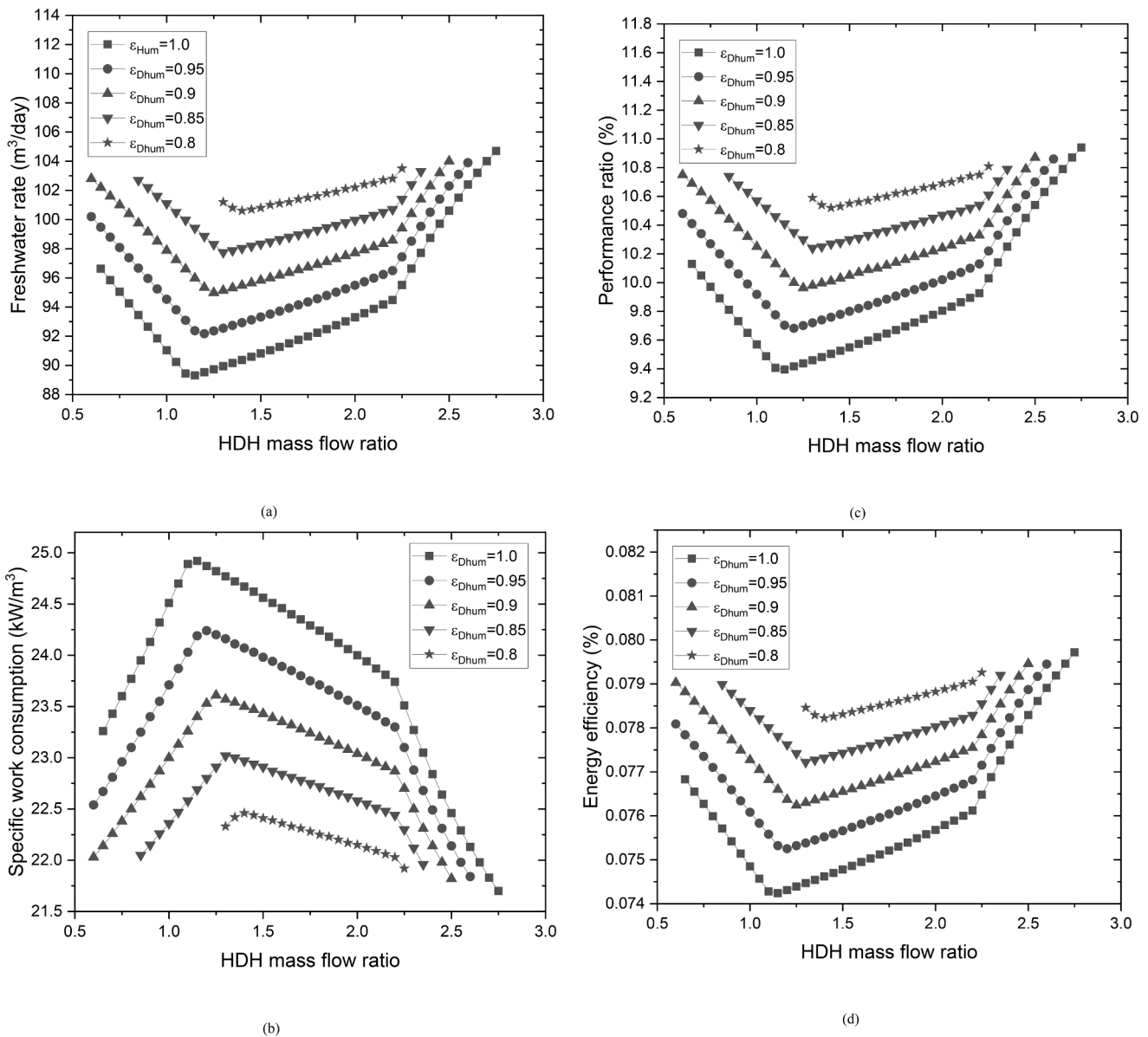


Fig. 6. Impact of HDH mass flow ratio on the: (a) freshwater rate, (b) specific work consumption, (c) performance ratio, (e) energy efficiency at different dehumidifier effectiveness levels. Square, circle, upward triangle, downward triangle, and star symbols represent value of humidifier effectiveness of 1.0, 0.95, 0.9, 0.85, and 0.8, respectively, while the value of humidifier effectiveness is fixed at 0.85.

concentrated saline water accumulated at the final stages of the MED-MVC unit to the HDH unit to achieve a minimal liquid discharge mechanism. This re-injection significantly increases the salinity of the rejected brine of the HDH unit, which is fed into the MED-MVC unit, which partly lowers the performance ratio of the MED-MVC unit. A decrease in the performance of the MED-MVC units reduces the water production capacity for the total hybrid desalination system.

As another significant metric, SWC increases with the rise of the HDH mass flow ratio at a range of approximately 0.5 to 1.5 and reaches its maximum of 22.85 kW/m^3 , 23.02 kW/m^3 , 23.17 kW/m^3 , 23.33 kW/m^3 , and 23.47 kW/m^3 for humidifier effectiveness of 0.8, 0.85, 0.9, 0.95, and 1.0, respectively. After that, the SWC decreases with the increase of the HDH mass flow ratio until it reaches its minimum value. Here, one of the crucial points regarding this trend is that the maximum and minimum performance metrics have occurred in different HDH mass flow ratio values. The lower the humidifier effectiveness, the earlier the turning point occurs, and the lower HDH mass flow ratios.

Fig. 6 presents alteration of the freshwater rate, SWC, performance

ratio, and energy efficiency versus the HDH mass flow ratio. In this figure, dehumidifier effectiveness is changing as well. It is noteworthy that square, circle, upward triangle, downward triangle, and star symbols represent the dehumidifier effectiveness values of 1.0, 0.95, 0.9, 0.85, and 0.8, respectively, while the value of humidifier effectiveness is fixed at 0.85. Net power and exergy efficiency are again excluded here due to their slight varying values. Like the alteration of the humidifier effectiveness, there are two different turning points in Fig. 6, which actually divide the charts into three different regions. The first region occurs in the lower HDH mass flow ratios (approximately less than 1.4). At this range, the freshwater rate, performance ratio, and energy efficiency decrease with the HDH mass flow ratio, while the SWC increases through this change. The value of the turning point at the end of the first region is decreased with the increase in the dehumidifier's effectiveness. Consequently, for different dehumidifier effectiveness values of 0.8, 0.85, 0.9, 0.95, and 1.0, the first turning point occurs in the HDH mass flow ratios of 1.4, 1.3, 1.25, 1.2, and 1.15, respectively.

In the second region, the freshwater rate, performance ratio, and

energy efficiency enhance with the HDH mass flow ratio increase until the second turning point appears. After the second turning point (third region), the parameters metrics sharply increased. On the other hand, the trend of the SWC is precisely opposite to that of the freshwater rate, performance ratio, and energy efficiency. Using rejected brine of HDH as a feed to the MED-MVC unit can reverse the alteration trends, in contrast to the alteration in the freshwater production rate seen in our previous studies (Rostami et al., 2021; Rostamzadeh et al., 2021). Also, the minimum values of freshwater rate, performance ratio, and energy efficiency occurred in higher dehumidifier effectiveness.

5. Concluding remarks

Employing a wind turbine to drive highly advanced desalination systems is a viable remedy for tackling water scarcity in the regions near open seas. However, such an idea can be matured by devising hybrid desalination systems driven by wind turbines' thermal and electrical energies. For the present study, the following concluding points can be drawn:

- The freshwater rate increased with the number of effects while the SWC decreased through this alteration.
- A seven-effect WT/HDH-MED-MVC system has a lower SWC than the base case.
- For wind speed values higher than 10 m/s, there was a sharp drop in energy and exergy efficiency values.
- In contrast with the SWC, there were decreasing and then increasing alterations in the freshwater rate, performance ratio, and energy efficiency with the rise of the HDH mass flow ratio.
- As a superior result, opting for the lowest value of humidifier/dehumidifier effectiveness can improve the performance of the WT/HDH-MED-MVC system.
- Among all components, the wind turbine had the highest exergy destruction rate of 6,967,000 W, followed by the heater (21,000 W).

Declaration of Competing Interest

The authors declare that they have no known competing financial interests or personal relationships that could have appeared to influence the work reported in this paper.

References

- Abdollahi Haghghi, M., Ghazanfari Holagh, S., Chitsaz, A., Parham, K., 2019. Thermodynamic assessment of a novel multi-generation solid oxide fuel cell-based system for production of electrical power, cooling, fresh water, and hydrogen. *Energy Convers. Manag.* 197, 111895 <https://doi.org/10.1016/j.enconman.2019.111895>.
- Bejan, A., Tsatsaronis, G., 1996. *Thermal Design and Optimization*. John Wiley & Sons.
- Ehyaei, M.A., Ahmadi, A., Rosen, M.A., 2019. Energy, exergy, economic and advanced and extended exergy analyses of a wind turbine. *Energy Convers. Manag.* 183, 369–381. <https://doi.org/10.1016/j.enconman.2019.01.008>.
- Elbassoussi, M.H., Antar, M.A., Zubair, S.M., 2021. Hybridization of a triple-effect absorption heat pump with a humidification-dehumidification desalination unit: thermodynamic and economic investigation. *Energy Convers. Manag.* 233, 113879 <https://doi.org/10.1016/j.enconman.2021.113879>.
- Elsayed, M.L., Mesalhy, O., Mohammed, R.H., Chow, L.C., 2019a. Transient and thermoeconomic analysis of MED-MVC desalination system. *Energy* 167. <https://doi.org/10.1016/j.energy.2018.10.145>.
- Elsayed, M.L., Mesalhy, O., Mohammed, R.H., Chow, L.C., 2019b. Performance modeling of MED-MVC systems: exergy-economic analysis. *Energy* 166. <https://doi.org/10.1016/j.energy.2018.10.080>.
- Elsayed, M.L., Mesalhy, O., Mohammed, R.H., Chow, L.C., 2018. Transient performance of MED processes with different feed configurations. *Desalination* 438, 37–53. <https://doi.org/10.1016/j.desal.2018.03.016>.
- Elsayed, M.L., Wu, W., Chow, L.C., 2021. High salinity seawater boiling point elevation: experimental verification. *Desalination* 504, 114955. <https://doi.org/10.1016/J.DESAL.2021.114955>.
- Fairuz, A., Faeshol Umam, M., Hasanuzzaman, M., Rahim, N.A., Mujtaba, I.M., 2023. Modeling and analysis of hybrid solar water desalination system for different scenarios in Indonesia. *Energy Convers. Manag.* 276, 116475 <https://doi.org/10.1016/J.ENCONMAN.2022.116475>.
- Ghiasirad, H., Asgari, N., Khoshbakhti Saray, R., Mirasoumi, S., 2021a. Geothermal-based freshwater production by humidification-dehumidification and evaporating desalination units integrated with a CCHP system: energy and exergy analysis. In: *International Conference on Desalination and Water Purification*. Amirkabir University of Technology, Bandarabas, Iran, p. 8 doi: ICDWP01.017.
- Ghiasirad, H., Asgari, N., Khoshbakhti Saray, R., Mirasoumi, S., 2021b. Thermoeconomic assessment of a geothermal based combined cooling, heating, and power system, integrated with a humidification-dehumidification desalination unit and an absorption heat transformer. *Energy Convers. Manag.* 235, 113969 <https://doi.org/10.1016/j.enconman.2021.113969>.
- Ghiasirad, H., Rostamzadeh, H., Nasri, S., 2020. Design and Evaluation of a New Solar Tower-Based Multi-generation System: part II, Exergy and Exergoeconomic Modeling. Integration of Clean and Sustainable Energy Resources and Storage in Multi-Generation Systems. Springer International Publishing, Cham, pp. 103–120. https://doi.org/10.1007/978-3-030-42420-6_6.
- Ghofrani, I., Moosavi, A., 2020. Energy, exergy, exergoeconomics, and exergoenvironmental assessment of three brine recycle humidification-dehumidification desalination systems applicable for industrial wastewater treatment. *Energy Convers. Manag.* 205, 112349 <https://doi.org/10.1016/j.enconman.2019.112349>.
- Ghorbani, B., Ebrahimi, A., Rooholamini, S., Ziabasharhagh, M., 2020. Pinch and exergy evaluation of Kalina/Rankine/gas/steam combined power cycles for tri-generation of power, cooling and hot water using liquefied natural gas regasification. *Energy Convers. Manag.* 223, 113328 <https://doi.org/10.1016/j.enconman.2020.113328>.
- International Energy Agency, 2020. *Renewables 2020. Analysis and Forecast to 2025*. Paris.
- Iranian Meteorological Organization (IMO), 2018. Available online: <http://www.irimo.ir/eng/index.php> (accessed on 30 June 2021). [WWW Document].
- Jamil, M.A., Zubair, S.M., 2018. Effect of feed flow arrangement and number of evaporators on the performance of multi-effect mechanical vapor compression desalination systems. *Desalination* 429. <https://doi.org/10.1016/j.desal.2017.12.007>.
- Jamil, M.A., Zubair, S.M., 2017a. On thermoeconomic analysis of a single-effect mechanical vapor compression desalination system. *Desalination* 420, 292–307. <https://doi.org/10.1016/j.desal.2017.07.024>.
- Jamil, M.A., Zubair, S.M., 2017b. Design and analysis of a forward feed multi-effect mechanical vapor compression desalination system: an exergo-economic approach. *Energy* 140. <https://doi.org/10.1016/j.energy.2017.08.053>.
- Javanfam, F., Ghiasirad, H., Khoshbakhti Saray, R., 2022. Efficiency Improvement and Cost Analysis of a New Combined Absorption Cooling and Power System. pp. 23–50. https://doi.org/10.1007/978-3-030-90720-4_2.
- Kalogirou, S.A., 2005. Seawater desalination using renewable energy sources. *Prog. Energy Combust. Sci.* 31, 242–281. <https://doi.org/10.1016/J.PECS.2005.03.001>.
- Karasu, H., Dincer, I., 2018. Analysis and Efficiency Assessment of Direct Conversion of Wind Energy Into Heat Using Electromagnetic Induction and Thermal Energy Storage. *J Energy Resour Technol* 140. <https://doi.org/10.1115/1.4039023>.
- Khalilzadeh, S., Hossein Nezhad, A., 2020. Using waste heat of high capacity wind turbines in a novel combined heating, cooling, and power system. *J Clean Prod* 276, 123221. <https://doi.org/10.1016/j.jclepro.2020.123221>.
- Khalilzadeh, S., Hossein Nezhad, A., 2018. Utilization of waste heat of a high-capacity wind turbine in multi effect distillation desalination: energy, exergy and thermoeconomic analysis. *Desalination* 439, 119–137. <https://doi.org/10.1016/j.desal.2018.04.010>.
- Lawal, D.U., Antar, M.A., Khalifa, A.E., 2021. Integration of a MSF Desalination System with a HDH System for Brine Recovery. *Sustainability* 13, 3506. <https://doi.org/10.3390/su13063506>.
- Memon, S., Lee, H.-S., Kim, W.-S., Kim, Y.-D., 2022a. Parametric investigation of modular configuration of multi-stage direct contact membrane distillation powered by waste heat of wind turbine. *Desalination* 533, 115770. <https://doi.org/10.1016/j.desal.2022.115770>.
- Memon, S., Lee, H.-S., Kim, W.-S., Kim, Y.-D., 2022b. Parametric investigation of modular configuration of multi-stage direct contact membrane distillation powered by waste heat of wind turbine. *Desalination* 533, 115770. <https://doi.org/10.1016/j.desal.2022.115770>.
- Narayan, G.P., Sharqawy, M.H., Lienhard V, J.H., Zubair, S.M., 2010. Thermodynamic analysis of humidification dehumidification desalination cycles. *Desalination Water Treat* 16, 339–353. <https://doi.org/10.5004/dwt.2010.1078>.
- Nayar, K.G., Sharqawy, M.H., Banchik, L.D., Lienhard V, J.H., 2016. Thermophysical properties of seawater: a review and new correlations that include pressure dependence. *Desalination* 390, 1–24. <https://doi.org/10.1016/j.desal.2016.02.024>.
- Nematollahi, O., Hajabdollahi, Z., Haghoooghi, H., Kim, K.C., 2019. An evaluation of wind turbine waste heat recovery using organic Rankine cycle. *J Clean Prod* 214. <https://doi.org/10.1016/j.jclepro.2019.01.009>.
- Okazaki, T., Shirai, Y., Nakamura, T., 2015. Concept study of wind power utilizing direct thermal energy conversion and thermal energy storage. *Renew Energy* 83, 332–338. <https://doi.org/10.1016/j.renene.2015.04.027>.
- Razmi, A., Soltani, M., Tayefeh, M., Torabi, M., Dusseault, M.B., 2019. Thermodynamic analysis of compressed air energy storage (CAES) hybridized with a multi-effect desalination (MED) system. *Energy Convers. Manag.* 199, 112047 <https://doi.org/10.1016/j.enconman.2019.112047>.
- Rostami, S., Rostamzadeh, H., Fatehi, R., 2021. A new wind turbine driven trigeneration system applicable for humid and windy areas, working with various nanofluids. *J Clean Prod* 296. <https://doi.org/10.1016/j.jclepro.2021.126579>.
- Rostamzadeh, H., 2021. A new pre-concentration scheme for brine treatment of MED-MVC desalination plants towards low-liquid discharge (LLD) with multiple self-superheating. *Energy* 225. <https://doi.org/10.1016/j.energy.2021.120224>.

- Rostamzadeh, H., Gargari, S.G., Namin, A.S., Ghaebi, H., 2018a. A novel multigeneration system driven by a hybrid biogas-geothermal heat source, Part I: thermodynamic modeling. *Energy Convers. Manag.* 177, 535–562. <https://doi.org/10.1016/j.enconman.2018.08.088>.
- Rostamzadeh, H., Ghiasirad, H., Amidpour, M., Amidpour, Y., 2020. Performance enhancement of a conventional multi-effect desalination (MED) system by heat pump cycles. *Desalination* 477. <https://doi.org/10.1016/j.desal.2019.114261>.
- Rostamzadeh, H., Namin, A.S., Ghaebi, H., Amidpour, M., 2018b. Performance assessment and optimization of a humidification dehumidification (HDH) system driven by absorption-compression heat pump cycle. *Desalination* 447. <https://doi.org/10.1016/j.desal.2018.08.015>.
- Rostamzadeh, H., Namin, A.S., Nourani, P., Amidpour, M., Ghaebi, H., 2019. Feasibility investigation of a humidification-dehumidification (HDH) desalination system with thermoelectric generator operated by a salinity-gradient solar pond. *Desalination* 462. <https://doi.org/10.1016/j.desal.2019.04.001>.
- Rostamzadeh, H., Rostami, S., 2020a. Performance enhancement of waste heat extraction from generator of a wind turbine for freshwater production via employing various nano fluids. *Desalination* 478, 114244. <https://doi.org/10.1016/j.desal.2019.114244>.
- Rostamzadeh, H., Rostami, S., 2020b. Performance enhancement of waste heat extraction from generator of a wind turbine for freshwater production via employing various nanofluids. *Desalination* 478. <https://doi.org/10.1016/j.desal.2019.114244>.
- Rostamzadeh, H., Rostami, S., Amidpour, M., He, W., Han, D., 2021. Seawater Desalination via Waste Heat Recovery from Generator of Wind Turbines: how Economical Is It to Use a Hybrid HDH-RO Unit? *Sustainability* 13 <https://doi.org/10.3390/su13147571>.
- Tahir, F., Al-Ghamdi, S.G., 2022. Integrated MED and HDH desalination systems for an energy-efficient zero liquid discharge (ZLD) system. *Energy Reports* 8, 29–34. <https://doi.org/10.1016/j.egy.2022.01.028>.
- Wepfer, W., WJ, W., RA, G., 1979. Proper evaluation of available energy for HVAC.
- Zaitsev, A., Mehrpooya, M., Ghorbani, B., Sanavbarov, R., Naumov, F., Shermatova, F., 2020. Novel integrated helium extraction and natural gas liquefaction process configurations using absorption refrigeration and waste heat. *Int. J. Energy Res.* 44, 6430–6451. <https://doi.org/10.1002/er.5377>.